An Innovative Method for the Sustainable Utilization of Blast-furnace Slag in the Cleaner Production of One-part Hybrid Cement

Esraa K. Fayed
Pyramids Higher Institution for Engineering and Technology
Fouad I. El-Hosiny
Ain Shams University
Ibrahim M. El-Kattan
Beni-Suef University
Hamdy A. Abdel-Gawwad (hamdyabdelgawwad@yahoo.com)
Housing and Building National Research Center (HBRC)

Research Article

Keywords: Blast-furnace slag, Sodium hydroxide, Chabazite, Activated species, Compressive strength

Posted Date: June 4th, 2021

DOI: https://doi.org/10.21203/rs.3.rs-581722/v1

Abstract

Hybrid cement (HC) can be defined as alkali activated-blended-Portland cement (PC). It was prepared by the addition of an alkaline solution to high-volume aluminosilicate-blended-PC. Although this cement exhibits higher mechanical performance compared to conventional blended one (aluminosilicate-PC blend), it represents lower commercial viability because of the corrosive nature of an alkaline solution. Therefore, this study focuses on the preparing one-part-HC using dry activator-based blast-furnace slag (DAS). DAS was prepared by mixing sodium hydroxide (NaOH) with blast-furnace slag (BFS) at low water to BFS ratio, followed by drying and grinding to yield DAS-powder. Different contents of DAS (equivalent to 70 wt.% BFS and 1, 2, and 3 wt.% NaOH) were blended with 30 wt.% PC. A mixture containing 70 wt.% BFS and 30 wt.% PC was used as a reference sample. The mortar was adjusted at sand: powder (BFS-PC and/or DAS-PC) weight ratio of 3: 1. The microstructural analysis proved that DAS-powder is mainly composed of sodium calcium aluminosilicate activated species and unreacted BFS. These species can interact again with water to form calcium aluminum silicate hydrate (C-A-S-H) and NaOH, suggesting that the DAS acts as NaOH-carrier. One-part HC-mortars having 1, 2, and 3 wt.% NaOH recorded 7-days compressive strength values 82, 44, and 27 %, respectively, higher than that of the control sample. At 180-days of curing, a significant reduction in compressive strength was observed within HC-mortar having 3 wt.% NaOH. This could be attributed to the increase of Ca (within C-S-H) replacement by Na, forming Na-rich-phase with lower binding capacity. The main hydration products within HC are C-S-H, C-A-S-H, and chabazite as one of zeolite family.

1. Introduction

Portland cement (PC) is the common and dominant binding material in the construction sector [1, 2]. Almost 4 billion tonnes is the annual production of PC worldwide, since China produces more than a half of global cement production [3, 4]. About 8% of the total anthropogenic global warming potential is resulted from PC-manufacturing [5]. Each metric tonne of PC requires 4.2 GJ energy, releasing approximately in 0.8-1.0 tonne of carbon footprint into surrounding environment [6]. To mitigate the high CO_2 emission and energy demand, several authors replaced a high portion of PC by supplementary cementitious materials such as fly ash (FA), silica fume (SF), and blast-furnace slag (BFS) [7–11]. Although the role of supplementary cementitious materials in the mitigation of carbon footprint and the improvement of the durability and the later mechanical properties of PC [12–17], the substitution of PC with high volume of these materials caused a noticeable retardation in its early hydration [18–20].

BFS is simply defined as a calcium aluminosilicate rich-waste resulted from the top of smelted iron during the heating of iron ore in a blast furnace. The molten BFS was quenched with water to yield glassy materials with high amorphous content [21]. Statistically, the extraction of 1 tonne of iron from ore generates almost 0.3 to 1.0 tonne BFS [22]. It is well known that BFS was used as a partial substituent to PC to yield what is called as slag cement [23]. Several authors stated that the replacement of PC by high volume BFS has reflected on a significant reduction of the heat of hydration, resulting in a retardation in the early compressive strength [24–26]. It was found that the performance and hydration characteristics of PC-BFS cement enhanced with increasing the curing temperature and the fineness of slag [27–29].

The addition of nano silica led to a significant improvement in the early compressive strength accompanied by an acceleration in setting time of high volume BFS blended cement [30–33]. A considerable improvement (16%) in the compressive strength of high volume BFS blended cement was achieved by the addition of 1 wt.% nano alumina [34]. the positive role of silica and alumina nano-particles is mainly originated from the formation of the additional

calcium silicate hydrate (C-S-H), ettringite and calcium aluminate hydrate (C-A-H), which have high efficiency in the mechanical properties improvement and the pore size reduction [30–34]. Other study [35] proved that the addition of 1 to 4 wt.% nano calcium carbonate to cement paste individually containing 70, 80, and 90 wt.% BFS led to the enhancement of their strengths by 8 to 24%, 1 to 16% and 2 to 20%, respectively.

As an innovative approach, the addition of alkalis to high volume BFS-blend-PC has resulted in the formation of the alkali-activated BSF-PC, namely hybrid cement (HC) [36, 37]. The individual addition of sodium hydroxide (NaOH) and sodium silicate (Na_2SiO_3) to PC containing 80 wt.% produced hardened materials with compressive strength value 4.5 and 10.8 times, respectively, higher than that BFS-PC blend [38]. After dissolving alkali, it should be kept for enough time to cool before its mixing with BFS-PC blend. The corrosive nature of alkaline solutions [39] is the common reason behind the retardation of the commercial viability of this type of cement. It is important to produce hybrid cement, in which alkali incorporated inside its composition. In other word, one-part-HC (just added water) should be prepared to achieve the safe use of this type of cement.

Therefore, this paper focused on the utilization of dry activator-based alkali activated BFS (DAS) in preparing one-part hybrid alkali-activated slag-PC. DAS was prepared by mixing sodium hydroxide solution with BFS (at low water to powder ratio of 0.1), followed by drying and grinding to yield DAS-powder, which acts as a safe and stable NaOH-carrier. The ability of sodium leaching from DAS into surrounding media was evaluated using pH measurement. The impact of sodium oxide content within dry activator on the performance of HC composed of 70 wt.% BFS and 30 wt.% PC was evaluated. This study also suggested the hydration reaction mechanism and the composition of strength-giving-phases resulted from one-part-HC.

2. Experimental

2.1. Materials resources

One-part hybrid cement (HC) mortar was fabricated from sand, ordinary Portland cement (OPC), blast-furnace slag (BFS), and sodium hydroxide (NaOH). Sand was brought from El-Wasta area (Beni Suef, Egypt). OPC (type I: 42.5 N) was purchased from Beni-Suef Cement Company (Cairo, Egypt). BFS was supplied from Helwan Company for Steel Industry (Helwan, Egypt). NaOH with purity of 99.99% was imparted by LOBA Chemical Company (India). Table 1 shows the chemical oxides compositions of OPC, BFS, and sand. X-ray diffraction (XRD) analysis (Fig. 1) proved that BFS exhibits a completely amorphous pattern with a hump at 2theta of 20–35º. OPC and BFS demonstrated specific surface areas of 3410 and 3540 cm^2/g, respectively.

2.2. Preparation of one-part hybrid cement powder

One-part hybrid cement powder was synthesized by mixing dry activator based alkali activated slag (DAS) with OPC. DAS was prepared by activating the BFS with NaOH solution, followed by drying and grinding. As shown in Table 2, BFS was individually activated by 1, 2, and 3 wt.% NaOH at W/BFS ratio of 0.1. The activated slurry immediately dried at 80 ºC for 24 h, followed by grinding to yield DAS-powder. The W/BFS ratio of 0.1 was chosen according to previously published work [40], which reported that W/BFS ratio of 0.1 is appropriate water content for the formation of alkali-activated powder with high capability to re-interact with water, yielding hardened materials. One-part-HC was prepared by mixing DAS with OPC at different weights equivalent to 70 wt. % BFS and 1, 2, and 3 % NaOH (by weight of BFS). Control sample containing 70 wt.% BFS and 30 wt.% OPC was made for comparison. The details of mixing proportions were listed in Table 3.

Table 1
Chemical oxides compositions of the starting raw materials

Samples notations	Chemical compositions, wt. %											
	SiO_2	CaO	MgO	Fe_2O_3	Al_2O_3	Na_2O	K_2O	Cl	SO_3	P_2O_5	TiO_2	LOI
OPC	21.01	63.15	2.45	3.36	5.09	0.37	0.07	0.04	2.69	-	-	1.82
BFS	41.51	34.58	4.59	0.57	13.38	1.94	0.86	0.06	1.73	0.32	0.43	-
Sand	94.38	-	-	1.21	2.17	0.12	0.09	0.03	0.09	0.02	0.04	0.13

Figure 1. XRD-pattern of blast-furnace slag (BFS)

Table 2
Compositions of the prepared dry activator based slag (DAS)

Dry activator notations	BFS	NaOH	Water content	Theoretical Wt. of DAS	Actual Wt. of DAS	NaOH within DAS powder	BFS, within DAS powder	Combined water within DAS powder
	Weight (gram)					Wt. %		
DAS-1	100.00	1.00	10.00	111.00	103.18	0.97	96.91	2.11
DAS-2	100.00	2.00	10.00	112.00	105.48	1.90	94.80	3.30
DAS-3	100.00	3.00	10.00	113.00	106.51	2.82	93.88	3.41

Table 3
Weights of BFS, OPC, and DAS within one-part-HC

Mixtures notations	BFS	OPC	DAS	Weight of BFS within DAS	Weight of NaOH within DAS
	Weight (gram)				
Control	70.00	30.00	-	-	-
HC-DAS-1	-	30.00	72.23	70.00	0.70
HC-DAS-2	-	30.00	73.84	70.00	1.40
HC-DAS-3	-	30.00	74.56	70.00	2.10

3.3. Preparation of one-part-HC mortar

One-part-HC mortar was designed at sand: powder (BFS-OPC and/or DAS-OPC) weight ratio of 3:1. Sand and powder were dry mixed in a ball mill; after that the dry blend was transferred to mixer, then the water was added (at W/P ratio of 0.47). Slow and rapid rates of wet mixing were applied on the fresh cement mortar to ensure the complete homogeneity. The workable mortar was transferred into stainless steel molds with dimensions 50 x 50 x 50 mm, followed by vibration, smoothing, and curing in relative humidity of 99 ± 1% at 23 ± 2 ºC for 24 h. Thereafter, the hardened mortar was demolded and cured under tap water for 7, 28, 90, and 180 days. Cement paste with the same BFS-OPC and DAS-OPC weight ratios were prepared for investigating the hydration products.

3.4. Experimental methods

Different experimental methods, including flowability, setting time, zeta potential, and compressive strength, were carried out on the prepared one-part-HC-paste and/or mortar. The workability of the fresh one-part-HC-mortar and BFS-OPC-mortar was determined by measuring the average spread diameters of the fresh mortar on flow the table [41]. Initial and final setting times of the fresh pastes were conducted three times on each mixture using Vicat apparatus based on ASTM C191 [42]. Zeta potential of the fresh cement mortars was measured using Malvern Zetasizer (nano-series), in which deionized water was used as a carrier liquid. This test was conducted to determine electrostatic repulsion between hydrated cement particles within cement mortar. Compressive strength of the hardened one-part-HC-mortar was measured according ASTM C109M [43] using German-Bruf-Pressing Machine with a maximum load capacity of 175kN. This test was conducted on three-hardened cubes of each mixture and the average reading was recorded. The broken paste was crushed and washed several times using acetone and methanol solution (at volume ratio of 1:1), then dried at 70 ºC for 3 h, to stop the hydration reaction. After that, the dried paste was kept in a vessel until analyses. In contrast, the broken cement mortar was immersed in the same solution for 24 h, followed by drying at 70 ºC for 3 h, and then kept until microstructural investigation.

3.5. Instrumental techniques

pH of the prepared DAS was conducted on the filtrate of the suspended solution (at DAS to distilled water weight ratio of 0.5) via Delta OHM HD 8705 pH meter and PCFC11 combination electrode with accuracy of 0.01. This test was conducted three times and the pH value was accepted if the variation rate of reading was less than 0.01 / minute. The oxides compositions of the starting materials were determined using X-ray fluorescence spectrometer (XRF: Xios, PW1400). The mineralogical compositions of the hardened cement pastes was identified using X-ray diffraction (XRD). This analysis was conducted on the powdered-sample of the hydrated cement pastes using Philips PW3050/60 diffractometer. The mineralogical compositions were determined within the 2theta range of 5–50º with 1s/step scanning rate and 0.05°/step resolution. Thermogravemetric analysis and its derivative (TG/DTG) was performed using DT-50 Thermal Analyzer (Schimadzu Co-Kyoto, Japan). This analysis was carried out on the powdered-cement paste to identify the hydration phases within its matrix. Each weight loss appeared at definite temperature is affiliated to the specific hydration product. This test was conducted by weighing 20 mg of sample in Pt-crucible, then heated in N_2 atmosphere up to 1000 ºC and heating rate of 10 ºC / min. The functional groups within hydration products were identified using Fourier transform infrared (FT-IR) spectroscopy (KBr-discussing Genesis-II FT-IR spectrometer) at the wavelength range of 400–4000 cm^{-1}. The microstructural development of the hardened one-part-HC-mortar was investigated using field emission scanning electron microscopy (FESEM, FEI Company, Holland) provided by an energy dispersive X-ray analyzer (EDS).

3. Results And Discussion

3.1. Characterization of DAS

The characterization of DAS is very important to determine its reaction mechanism and its role in the hydration of one-part-HC. FESEM-micrographs (Fig. 2) show that the addition of NaOH to BFS during preparing DAS has resulted in a partial dissolution of polygonal-shaped-BFS particle to form sodium calcium aluminosilicate species as confirmed by EDS-analysis. Additionally, the formation of these species enhances with NaOH addition.
As stated by Davidovits [44], gehlenite and akermanite within BFS can be dissolved by NaOH to yield (Na, Ca)-ortho-sialate hydrate and calcium silicate hydrate as activated species. After that, these species condense together to form (Na, Ca)-cyclo-ortho-(sialate-disiloxo) and excess of calcium silicate hydrate (Fig. 3). Polymerization process is the following step, in which a long chain of sodium calcium aluminosilicate is formed. The mixing

water content plays an important role in the dissolution/condensation process [45]. As prviously stated [40], the use of low water during activation process plays a circular role in the control of condensation rate. The addition of low water content, followed by drying, causes a retardation in the condensation process, forming DAS with high activated species content. This is the main reason behind the justification of mixing water at W/BFS ratio of 0.1 and the application of drying during preparing DAS.

To identify the reactivity of activated species, the leaching test was applied to the prepared DAS. As shown in Fig. 4, a significant rising in pH-value in a short time (5 minutes) was recorded after suspension of DAS-powder in water. The possible explanation of this outcome is the moving Na cation at the ortho position within activated species, forming sodium hydroxide in the water medium (Fig. 5). This means the high hydraulic reactivity of DAS, as the activation process can be continued after water addition. It can be said that the DAS acts as a carrier of NaOH, which strongly contributes to resolve the corrosive nature of alkali solutions during preparing one-part-HC.

3.2. Flowability and zeta potential of one-part-HC-mortars

The impact of NaOH contents within DAS on the workability and zeta potential of fresh one-part-HC mortar is represented in Fig. 6. Generally, the spreading diameter of the fresh HC-mortars indicates their workability. The fresh HC-mortar with the broadest speeding diameter exhibits the best fluidity. There is a direct relationship between the flowability of the mortar and the negative zeta potential values. Increasing the NaOH content within DAS leads to a significant enhancement in the workability, which coincides with an increment in negative zeta potential value, as in line with the previously published work [46], which stated that the addition of Na_2O content enhances the workability of one-part alkali activated cement. He et al. [47] proved that increasing negative zeta potential is mainly originated from an increment in the electrostatic repulsive force between cement particles, resulting in an enhancement in the workability of the fresh cementitious material.

3.3. Setting time of one-part-HC pastes

The initial and final setting times (IST and FST, respectively) of the fresh BFS-OPC and DAS-OPC pastes are shown in Fig. 7. The setting time of the fresh cement paste mainly depends on the content of NaOH within DAS. Depending on the composition of the fresh cement pastes, the IST was identified after 183-264 minute; meanwhile, the FST was recorded after 275-367 minute. One-part HC samples record shorter IST and FST compared to BFS-OPC blend. The setting time decreases toward control > HC-DAS-1 > HC-DAS-2 > HC-DAS-3. This means that increasing NaOH content has a significant effect on the dissolution of aluminosilicate and the formation of binding phases [48].

3.4. Phase identification

The XRD-patterns of the BFS-PC blend (reference sample) and one-part HC-pastes hydrated for 7 and 28-days are shown in Fig. 8. Portlandite ($Ca(OH)_2$), C-S-H, calcite, and ettringite are the main phases within control sample. Beside ($Ca(OH)_2$), C-S-H, calcite peaks, chabazite (calcium sodium aluminum silicate hydrate: C-N-A-S-H) and gypsum were identified within the patterns referred to one-part HC-pastes. For both control and one-part HC-DAS-2 mixtures, increasing curing times from 7 up to 28 days results in a significant depletion of $Ca(OH)_2$ accompanied by an enhancement in C-S-H growth. This confirmed the improvement of pozzolanic rate with time advanced, similar to the previous works [49-51]. Nevertheless, one-part HC-DAS-2 demonstrated the highest $Ca(OH)_2$ consumption and C-S-H formation rates. Increasing NaOH content up to 3 wt.% within DAS has resulted in a

significant increment in C-S-H formation at the expense of $Ca(OH)_2$ phase. This confirms the fact that the activated aluminosilicate species within DAS can easily interact with $Ca(OH)_2$ to yield C-S-H and/or C-N-A-S-H binding phases [52-55]. Ettringite has been detected within the pattern affiliated to control sample at 7-days of hydration. With time advanced up to 28 days, ettringite peaks disappeared. This confirmed the dissociation of ettringite with curing time, as in agreement with previous reports [23, 56]. On the other hand, the presence of alkali within one-part HC-paste prevents the formation of ettringite. This could be the possible reason behind the appearance of gypsum within the hydrated one-part HC pastes. Halaweh [57] stated that the presence of alkali increases the rate of sulfate release into solution, causing instability of ettringite.

Fig. 9 represents the TG/DTG-curves of BFS-OPC blend and one-part-HC hydrated for 7 and 28-days. All peaks are mainly related to the weight loss of the hydration phases within hardened pastes. The compositions of the hydration products strongly depend on the temperature at which the peak appeared. The peaks appeared at the temperature range of 50-200 ºC are mainly affiliated to the dehydration of combined water within C-S-H, C-A-S-H, and/or C-N-A-S-H [58, 59]. Other peaks at 487 ºC are related to the decomposition of $Ca(OH)_2$ [60, 61]. The peaks referred to the decarbonation of $CaCO_3$ were identified at a temperature range of 600-800 ºC [62, 63].

For BFS-OPC and one-part HC-DAS-2 mixtures, increasing curing time causes an enhancement in the intensity of C-S-H, C-A-S-H and/or C-N-A-S-H peaks at the expense of $Ca(OH)_2$. This perfectly highlights the fact that the activation, hydration, and pozzolanic reactions are ongoing with time advanced. Comparing with the reference sample, the HC-DAS-2 mixture demonstrates the higher C-S-H, C-A-S-H and/or C-N-A-S-H peaks intensity at 7 and 28 days of curing. This confirms the positive role of Na_2O within DAS in the acceleration of the pozzolanic reaction and the formation of excessive binding-phases content. As aforementioned, the DAS is mainly composed of reactive sodium calcium aluminosilicate species. These activated species can hydrate and interact with $Ca(OH)_2$, to yield binding-phases easier than gehlenite and akermanite mineral within BFS. Increasing NaOH content up to 3 wt.% (HC-DAS-3) enhanced the formation of C-S-H, C-A-S-H and/or C-N-A-S-H accompanied by a significant consumption of $Ca(OH)_2$. These outcomes agree with XRD-results.

3.5. Compressive strength

The compressive strength values of the hardened BFS-OPC and one-part-HC-mortars are graphically represented in Fig. 10. Increasing curing time (up to 180 days) was found to have a positive impact on the compressive strength development. This means the successive formation of strength-giving-phases (C-S-H C-A-S-H, and/or C-N-A-S-H) with time advanced as confirmed by XRD and TG/DTG analyses. Same trend was observed in the previously published reports [37, 64-65]. Increasing NaOH content within DAS up to 2 wt. % materially improves the early compressive strength (at 7-days). The NaOH-content beyond 2 wt.% reduces 7-days compressive strength, but still higher than that of the control sample (BFS-OPC). One-part-HC-mortars individually containing DAS-1, DAS-2, and DAS-3 exhibit 7-days compressive strength ~ 44, 77, and 27 %, respectively, higher than that of the hardened BFS-OPC mortar. At later ages (28 to 180-days), the HC-DAS-1 and HC-DAS-2 show the same trend. The hardened HC-DAS-3 achieves later compressive strengths lower than those of the control sample. This proves the fact that the NaOH-content released from DAS (Fig. 5) plays an important role in the performance of one-part HC-mortar.

Cement hydration and alkali BFS activation are the two synergistic mechanisms of one-part HC-mortar. The activated aluminosilicate species-containing-DAS interacts with water to yield C-A-S-H and NaOH (Fig. 5). The unreacted BFS within DAS was dissolved by the liberated NaOH through alkali-activation process, yielding C-N-A-S-

H, as confirmed by XRD-analysis (Fig. 8). On the other hand, the OPC within one-part HC-mortar also interacts with water to produce C-S-H and $Ca(OH)_2$. An additional C-N-A-S-H could be formed through the consumption of $Ca(OH)_2$ by the activated species resulted from alkali BFS-activation. In contrast, the formation of strength-giving-phases is resulted from the pozzolanic reaction, as C-S-H and/or C-A-S-H, was formed through the interaction between aluminosilicate within BFS and $Ca(OH)_2$ resulted from OPC hydration.

It is recognized that the enhancement of hydration products' content strongly reflects on the mechanical properties of the hydrated cement [40, 46, 58, 66, 67]. Accordingly, a relationship between compressive strength and hydration products content (determined by TG-analysis) within cement pastes hydrated for 28-days was represented in Fig.11. Increasing NaOH content (up to 2 wt. %) enhances formation of the hydration products and compressive strength. Although the hydrated sample having 3 wt. % exhibits the highest hydration products content, it demonstrated compressive strength value lower than those of other HC-mixtures and control sample. These variations in outcomes confirm the fact that the DAS with appropriate Na_2O content should be prepared to achieve the high performance of one-part HC.

As suggested by Shi et al. [68], the Na_2O could interact with C-S-H through different three mechanisms. The neutralization of acidic silanol group (Si-OH) is the possible first reaction. The second mechanism includes the partial replacement of Ca ion in C-S-H to yield N-C-S-H. Meanwhile, the third mechanism is the formation of $Si—O^-Na^+$ through the complete destruction of the binding capacity of C-S-H. It can be said that these mechanisms mainly depend on the content of Na_2O in the cement matrix. The first and second mechanisms happen in the presence of relatively low Na_2O content; whereas the third occurs at the high Na_2O content. For HC-DAS-1 and HC-DAS-2 mixtures, the appropriate Na_2O-content leads to the formation of N-C-A-S-H accompanied by compressive strength development. Conversely, a competition between second and third mechanism could happen in with HC-DAS-3 mixture, resulting in the formation of hydration products with lower binding capacity compared with those of other samples.

3.6. Microstructure

Fig. 12 displayed the FESEM-micrographs and elemental EDS-patterns of control and one-part HC-mortars. For BFS-OPC and HC-DAS-2 mixtures, increasing curing time from 7 up to 28-days enhanced the compaction of microstructure and the formation of binding phases, confirming the compressive strength results. At 7-days of curing, the flakey-shaped-phase is the dominant hydration product within BFS-OPC mixture. With time advanced (up to 28-days), this phase transformed to interconnected fiber-shaped-phase. The EDS-analysis confirmed that these phases (flakey- and fiber-shaped-phases) are mainly affiliated to C-S-H and/or C-A-S-H. No transformation in the morphology of hydration products has been detected with curing time of HC-DAS-2. Nonetheless, increasing curing time caused an enhancement in the formation of needle-C-S-H and rhombohedral zeolitic chabazite (C-N-A-S-H) crystals, as proved by EDS-analysis. This is in line with XRD-results. Additionally, same morphology of chabazite phase has been identified in the previously published works [69-71]. Finally, needle-shaped-crystals and minor of rhombohedral-chabazite-crystals were distributed on gel-like phase within the microstructure of HC-DAS-3 mixture hydrated for 28-days. These variations in the microstructural development and the morphology of the hydration products proved the role of Na_2O content in the mechanical performance of the prepared one-part HC-mortars. Therefore, a relationship between Na/Ca ratio (identified by EDS-analysis) and 28-days compressive strength values of one-part HC-mortar was represented in Fig. 13. Increasing the NaOH within DAS induces the incorporation of Na into the hydration products. In other words, the replacement of Ca within C-S-H and/or C-A-S-H

enhanced with NaOH addition. Interestingly, the best 28-days compressive value was recorded at Na/Ca mole ratio of 0.11. Whereas a significant regression in compressive strength values was achieved when the NaOH content within DAS increases up to 3 wt.%.

4. Conclusions

This paper reported the synthesis and characterization of one-part hybrid cement mortar, in which dry activator-based blast-furnace slag and Portland cement were the main ingredients. Dry activator with different contents were blended with Portland cement to achieve 70 wt.% blast-furnace slag and 1, 2, 3 wt.% NaOH. The hydrated one-part hybrid cement mortar containing 1 and 2 wt.% NaOH was found to exhibit shorter setting time, higher workability, and higher compressive strength compared to blended cement containing the same blast-furnace slag content. Although incorporating dry activator content equivalent to 3 wt.% NaOH accelerated the setting time and enhanced the workability and early compressive strength, it demonstrated the lower compressive strength at later ages of curing. Accordingly, sodium hydroxide content within dry activator played an important role in the performance of the prepared mortar, especially at later ages of hydration. As suggested by the reaction mechanism, dry activator is mainly composed of sodium calcium aluminosilicate species with a high ability to re-interact with water, yielding calcium aluminum silicate hydrate and sodium hydroxide. The liberated sodium hydroxide accelerated the dissolution of unreacted slag particles, resulting in an acceleration in the hydration products formation which coincided with compressive strength improvement. As identified by X-ray diffraction and thermogravemetric analyses, calcium silicate hydrate, calcium aluminum silicate hydrate, and chabazite zeolite are the dominant hydration products with the prepared hybrid cement. It can be said that preparatig dry activator resolved the drawback of the corrosive nature of alkaline solution, which could strongly reflect on the safe use of hybrid cement in different construction projects.

References

1. M. Juenger, F. Winnefeld, J. Provis, J. Ideker, Advances in alternative cementitious binders, Cement and Concrete Research. 41 (2011) 1232–1243. http://dx.doi.org/10.1016/j.cemconres.2010.11.012
2. P. A. Claisse, Introduction to cement and concrete, Civil Engineering Materials, Butterworth-Heinemann (2016) 155–162. https://doi.org/10.1016/C2014-0-03170-X
3. M. Garside, Major countries in worldwide cement production 2015–2019, Statista. (2020).https://www.statista.com/statistics/267364/world-cement-production-by-country/
4. DATIS Export Group, July 2020. Worldwide Cement Production from 2015 to 2019. https://datis-inc.com/blog/worldwide-cement-production-from-2015-to-2019/#Worldwide_Cement_Production_from_2015_to_2019
5. R. M. Andrew, Global CO_2 emissions from cement production, Earth System Science Data 10 ((2018) 195–217.
6. E. Gartner, Industrially interesting approaches to “low-CO2” cements, Cement and Concrete Research. 34 (2004) 1489–1498.
7. M. A. Sanjuan, C. Argiz, J. C. Gálvez, A. Moragues, Effect of silica fume fineness on the improvement of Portland cement strength performance, Construction and Building Materials 96 (2015) 55–64.
8. Y. Jeong, S. H. Kang, M. O. Kim, J. Moon, Acceleration of cement hydration by hydrophobic effect from supplementary cementitious materials: Performance comparison between silica fume and hydrophobic silica,

Cement and Concrete Composites 112 (2020) 103688.

9. S. Gupta, H. W. Kua, Combination of biochar and silica fume as partial cement replacement in mortar: performance evaluation under normal and elevated temperature, Waste and Biomass Valorization 11(6) (2020) 2807–2824.
10. P. Tang, W. Chen, D. Xuan, Y. Zuo, C. S. Poon, Investigation of cementitious properties of different constituents in municipal solid waste incineration bottom ash as supplementary cementitious materials, Journal of Cleaner Production 258 (2020) 120675.
11. R. A. Rivera, M. Á. Sanjuán, D. A. Martín, Granulated blast-furnace slag and coal fly ash ternary Portland cements optimization, Sustainability 12(14) (2020) 5783.
12. S. A. Miller, Supplementary cementitious materials to mitigate greenhouse gas emissions from concrete: can there be too much of a good thing?, Journal of Cleaner Production 178 (2018) 587–598.
13. J. Zhang, Q. Wang, Z. Wang, Optimizing design of high strength cement matrix with supplementary cementitious materials, Construction and building materials 120 (2016) 123–136.
14. X. Lv, Y. Dong, R. Wang, C. Lu, X. Wang, Resistance improvement of cement mortar containing silica fume to external sulfate attacks at normal temperature, Construction and Building Materials 258, (2020) 119630.
15. M. S. Nasr, T. Hussain, H. Kubba, A. A. F. Shubbar, Influence of using high volume fraction of silica fume on mechanical and durability properties of cement mortar, Journal of Engineering Science and Technology 15(4) (2020) 2494–2506.
16. A. K. Saha, P. K. Sarker, Effect of sulphate exposure on mortar consisting of ferronickel slag aggregate and supplementary cementitious materials, Journal of Building Engineering 28 (2020) 101012.
17. D. J. D. Souza, M. H. F. D. Medeiros, J. Hoppe Filho, Evaluation of external sulfate attack (Na2SO4 and MgSO4): Portland cement mortars containing siliceous supplementary cementitious materials, Revista IBRACON de Estruturas e Materiais 13(4) (2020) 1–16.
18. Z. Yingliang, Q. Jingping, M. A. Zhengyu, G. Zhenbang, L. Hui, Effect of superfine blast furnace slags on the binary cement containing high-volume fly ash, Powder Technology 375 (2020) 539–548.
19. A. B. Harwalkar, S.S. Awanti, Laboratory and field investigations on high-volume fly ash concrete for rigid pavement, Transp. Res. Rec. 2441 (2014)121–127.
20. Y. Yao, J.K. Gong, Z. Cui, Anti-corrosion performance and microstructure analysis on a marine concrete utilizing coal combustion byproducts and blast furnace slag, Clean. Technol. Environ. Policy 16 (2013) 545–554.
21. J.L. Provis, A. Palomo, C. Shi, Advances in understanding alkali-activated materials, Cement and Concrete Research 78 (2015) 110–125.
22. Lei Wang, Liang Chen, Daniel C. W. Tsang, Green remediation by using low-carbon cement-based stabilization/solidification approaches, D. Hou (Ed.), Sustainable Remediation of Contaminated Soil and Groundwater: Materials, Processes, and Assessment. Butterworth-Heinemann (2019) 93–118.
23. P. C. Hewlett, M. Liska, Lea's Chemistry of Cement and Concrete, fifth ed., Edward Arnold Ltd., London, 2019.
24. B. Kolani, L. Buffo-Lacarrière, A. Sellier, G. Escadeillas, L. Boutillon, L. Linger, Hydration of slag-blended cements, Cement and Concrete Composites 34(9) (2012) 1009–1018.
25. K. Sakai, H. Watanabe, M. Suzuki, K. Hamazaki, Properties of granulated blast-furnace slag cement concrete, In: Istanbul Conference 132 (1992) 1367–83.

26. H. Binici, H. Temiz, M.M. Kose, The effect of fineness on the properties of the blended cements incorporating ground granulated blast furnace slag and ground basaltic pumice, Cem Concr Res. 21 (2007) 1122–1128.
27. J. I. Escalante, L. Y. Gomez, K. K. Johal, G. Mendoza, H. Mancha, J. Mendez, Reactivity of blast-furnace slag in Portland cement blends hydrated under different conditions, Construction and Building Materials 31 (2001) 1403–1409.
28. H. Binici, H. Temiz, M. M. Köse, The effect of fineness on the properties of the blended cements incorporating ground granulated blast furnace slag and ground basaltic pumice, Construction and Building Materials 21(5) (2007) 1122–1128.
29. J. Zhu, Q. Zhong, G. Chen, D. Li, Effect of particlesize of blast furnace slag on properties of portland cement, Procedia Engineering 27 (2012) 231–236.
30. M. H. Zhang, J. Islam, S. Peethamparan, Use of nano-silica to increase early strength and reduce setting time of concretes with high volumes of slag, Cement and Concrete Composites 34(5) (2012) 650–662.
31. M. H. Zhang, J. Islam, Use of nano-silica to reduce setting time and increase early strength of concretes with high volumes of fly ash or slag, Construction and Building Materials 29 (2012) 573–580.
32. F. U. A. Shaikh, A. Hosan, Effect of nano silica on compressive strength and microstructures of high volume blast furnace slag and high volume blast furnace slag-fly ash blended pastes, Sustainable Materials and Technologies 20 (2019) e00111.
33. W. Jiang, X. Li, Y. Lv, D. Jiang, Z. Liu, C. He, Mechanical and hydration properties of low clinker cement containing high volume superfine blast furnace slag and nano silica, Construction and Building Materials 238 (2020) 117683.
34. F. U. A. Shaikh, A. Hosan, Effect of nano alumina on compressive strength and microstructure of high volume slag and slag-fly ash blended pastes, Frontiers in Materials 6 (2019) 90.
35. A. Hosan, F. U. A. Shaikh, Influence of nano-CaCO3 addition on the compressive strength and microstructure of high volume slag and high volume slag-fly ash blended pastes, Journal of Building Engineering 27 (2020) 100929.
36. I. Amer, M. Kohail, M. S. El-Feky, A. Rashad, M. A. Khalaf, Characterization of alkali-activated hybrid slag/cement concrete, Ain Shams Engineering Journal 12 (2021) 135–144.
37. S. Shagñay, L. Ramón, M. Bautista, A. Fernández-Álvarez, F. Velasco, M. Torres-Carrasco, Eco-Efficient Hybrid Cements: Pozzolanic, Mechanical and Abrasion Properties, Applied Sciences 10(24) (2020) 8986.
38. D. E. Angulo-Ramírez, R. M. de Gutiérrez, F. Puertas, Alkali-activated Portland blast-furnace slag cement: Mechanical properties and hydration, Construction and Building Materials 140 (2017) 119–128.
39. J. Davidovits, Development of user-friendly systems In: Geopolymer chemistry and applications, 5th edition, Institut Géopolymère Saint-Quentin, France (2020) 475–481.
40. H. A. Abdel-Gawwad, S. Abd El-Aleem, A.S. Ouda, Preparation and characterization of one-part non-Portland cement, Ceramics International 42(1) (2016) 220–228.
41. ASTM C230/C230M, 2014. Standard Specification for flow table for use in tests of hydraulic cement.
42. ASTM C191, 2018. Standard Test Methods for Time of Setting of Hydraulic Cement by Vicat Needle.
43. ASTM C109/C109M, 2020. Standard Test Method for Compressive Strength of Hydraulic Cement Mortars.
44. J. Davidovits, Calcium based geopolymer, (Ca, K, Na)-sialate, Si: Al = 1, 2, 3. In: Geopolymer chemistry and applications. 5th edition, Institut Géopolymère Saint-Quentin, France, (2020) 209–246.

45. Z. Zuhua, Y. Xiao, Z. Huajun, C. Yue, Role of water in the synthesis of calcined kaolin-based geopolymer, Applied Clay Science 43(2) (2009) 218–223.
46. H. A. Abdel-Gawwad, M.S. Mohammed, E.N. Ads, A novel eco-sustainable approach for the cleaner production of ready-mix alkali activated cement using industrial solid wastes and organic-based activator powder, Journal of Cleaner Production 256 (2020) 120705.
47. Y. He, X. Zhang, R.D. Hooton, Effects of organosilane-modified polycarboxylate superplasticizer on the fluidity and hydration properties of cement paste, Construction and Building Materials. 132 (2017) 112–123.
48. J. Yliniemi, B. Walkley, J. L. Provis, et al., Influence of activator type on reaction kinetics, setting time, and compressive strength of alkali-activated mineral wools, J Therm Anal Calorim (2020). https://doi.org/10.1007/s10973-020-09651-6.
49. Y. Elakneswaran, E. Owaki, S. Miyahara, M. Ogino, T. Maruya, T. Nawa, Hydration study of slag-blended cement based on thermodynamic considerations, Construction and building materials 124 (2016) 615–625.
50. Y. Liu, S. Lei, M. Lin, Y. Li, Z. Ye, Y. Fan, Assessment of pozzolanic activity of calcined coal-series kaolin, Applied Clay Science 143 (2017) 159–167.
51. Y. Zhao, J. Gao, C. Liu, X. Chen, Z. Xu, The particle-size effect of waste clay brick powder on its pozzolanic activity and properties of blended cement, Journal of Cleaner Production 242 (2020) 118521.
52. A. Fernández-Jiménez, F. Zibouche, N. Boudissa, I. García-Lodeiro, M. T. Abadlia, A. Palomo, Metakaolin-Slag-Clinker Blends, The role of Na + or K + as alkaline activators of these ternary blends, J. Am. Ceram. Soc. 96 (6) (2013) 1991–1998.
53. I. Garcia-Lodeiro, A. Fernández-Jiménez, A. Palomo, Variation in hybrid cements over time. Alkaline activation of fly ash-portland cement blends, Cem. Concr. Res. 52 (2013) 112–122.
54. I. Garcia-Lodeiro, A. Fernández-Jiménez, A. Palomo, Hydration kinetics in hybrid binders: Early reaction stages, Cem. Concr. Compos. 39 (2013) 82–92.
55. I. Garcia-Lodeiro, S. Donatello, A. Fernández-Jiménez, Á. Palomo, Hydration of hybrid alkaline cement containing a very large proportion of fly ash: a descriptive model, Materials 9(7) (2016) 605.
56. M. Fridrichová, K. Dvolák, D. Gazdic, J. Mokrá, K. Kulísek,Thermodynamic Stability of Ettringite Formed by Hydration of Ye'elimite Clinker, Advances in Materials Science and Engineering. 2016 (2016) 9280131. https://doi.org/10.1155/2016/9280131
57. M. A. Halaweh, Effect of alkalis and sulfates on Portland cement systems. Ph.D. thesis, University of South Florida, USA. 2006.
58. H. A. Abdel-Gawwad, M. S. Mohammed, T. Alomayri, Single and dual effects of magnesia and alumina nano-particles on strength and drying shrinkage of alkali activated slag, Construction and Building Materials 228 (2019) 116827.
59. E. L'Hôpital, B. Lothenbach, D.A. Kulik, K. Scrivener, Influence of calcium to silica ratio on aluminium uptake in calcium silicate hydrate,Cement and Concrete Research 85 (2016) 111–121.
60. D. Jiang, X. Li, Y. Lv, M. Zhou, C. He, W. Jiang, Z. Liu, C. Li, Utilization of limestone powder and fly ash in blended cement: Rheology, strength and hydration characteristics, Construction and Building Materials 232 (2020) 117228.
61. Z. Wu, Y. Wei, S. Wang, J. Chen, Application of X-ray micro-CT for quantifying degree of hydration of slag-blended cement paste, Journal of Materials in Civil Engineering 32(3) (2020) 04020008.

62. Z.X. Chen, S.H. Chu, Y.S. Lee, H.S. Lee, Coupling effect of γ-dicalcium silicate and slag on carbonation resistance of low carbon materials, Journal of Cleaner Production 262 (2020) 121385.
63. J. Zhang, C. Shi, Z. Zhang, Effect of Na2O concentration and water/binder ratio on carbonation of alkali-activated slag/fly ash cements, Construction and Building Materials 269 (2020) 121258.
64. I. Garcia-Lodeiro, N. Boudissa, A. Fernández-Jiménez, A. Palomo, Use of clays in alkaline hybrid cement preparation. The role of bentonites, Materials Letters 233 (2018) 134–137.
65. Z. Abdollahnejad, P. Hlavacek, S. Miraldo, F. Pacheco-Torgal, J. L. B. D. Aguiar, Compressive strength, microstructure and hydration products of hybrid alkaline cements, Materials Research 17(4) (2014) 829–837.
66. H. A. Abdel-Gawwad, S. V. García, H. S. Hassan, Thermal activation of air cooled slag to create one-part alkali activated cement, Ceramics International 44(12) (2018) 14935–14939.
67. H. A. Abdel-Gawwad, S. A. Mohamed, M. S. Mohammed, Recycling of slag and lead-bearing sludge in the cleaner production of alkali activated cement with high performance and microbial resistivity,Journal of Cleaner Production 220 (2019) 568–580.
68. C. Shi, P. V. Krivenko, D. Roy, Alkali-Activated slag cement and concrete. In: Hydration and microstructure of alkali activated slag cement, Taylor & Francis, USA. (2006) 64–276.
69. Y. Hasegawa, H. Hotta, K. Sato, T. Nagase, F. Mizukami, Preparation of novel chabazite (CHA)-type zeolite layer on porous α-Al2O3 tube using template-free solution, Journal of membrane science 347(1–2) (2010) 193–196.
70. N. Zhang, Y. Xin, Q. Li, X. Ma, Y. Qi, L. Zheng, Z. Zhang, Ion Exchange of One-Pot Synthesized Cu-SAPO-44 with NH4NO3 to Promote Cu Dispersion and Activity for Selective Catalytic Reduction of NOx with NH3, Catalysts 9(11) (2019) 882.
71. A. Nearchou, A. Sartbaeva,Influence of alkali metal cations on the formation of zeolites under hydrothermal conditions with no organic structure directing agents, Cryst. Eng. Comm. 17(12) (2015) 2496–2503.

Figures

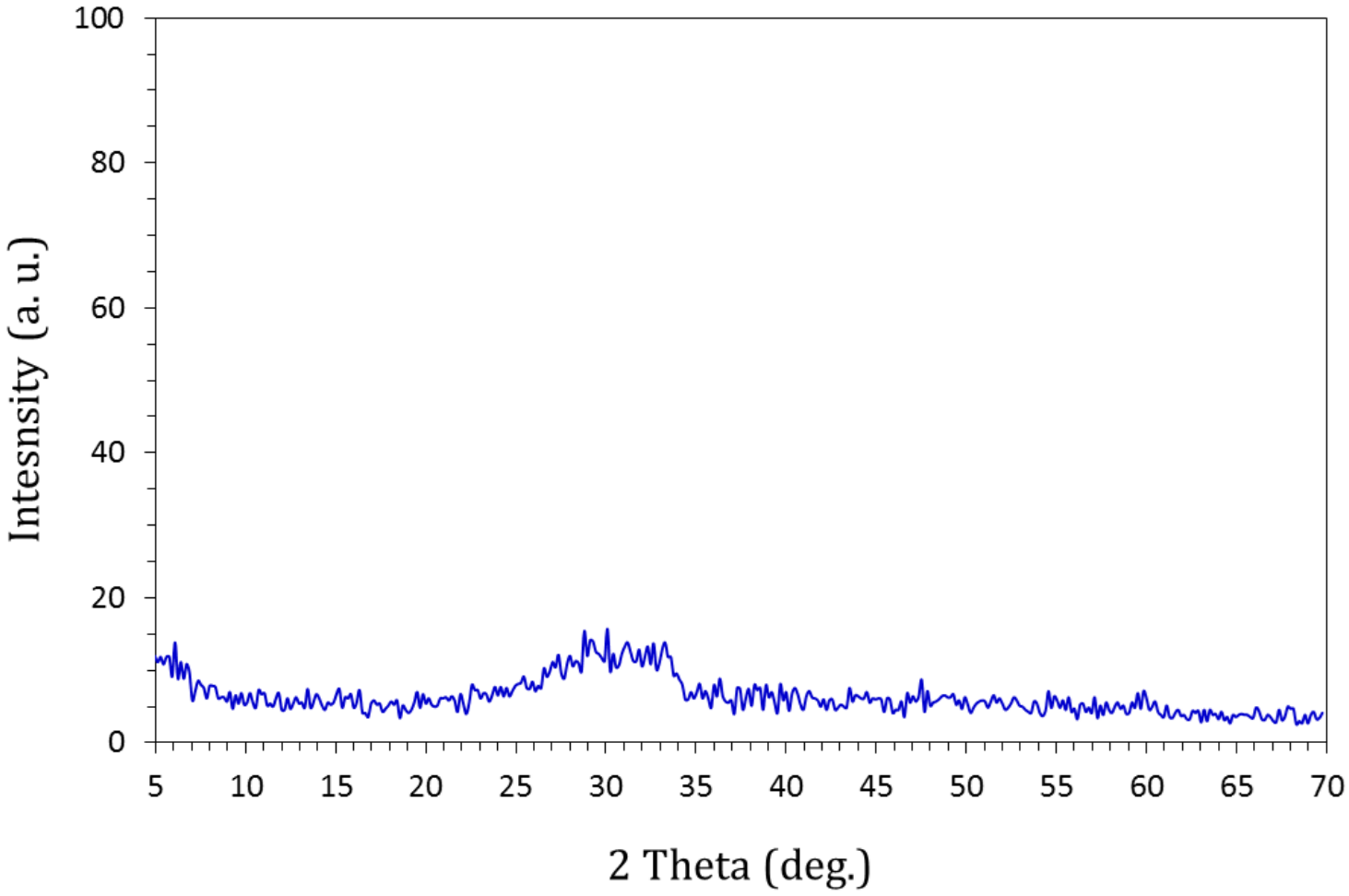

Figure 1

XRD-pattern of blast-furnace slag (BFS)

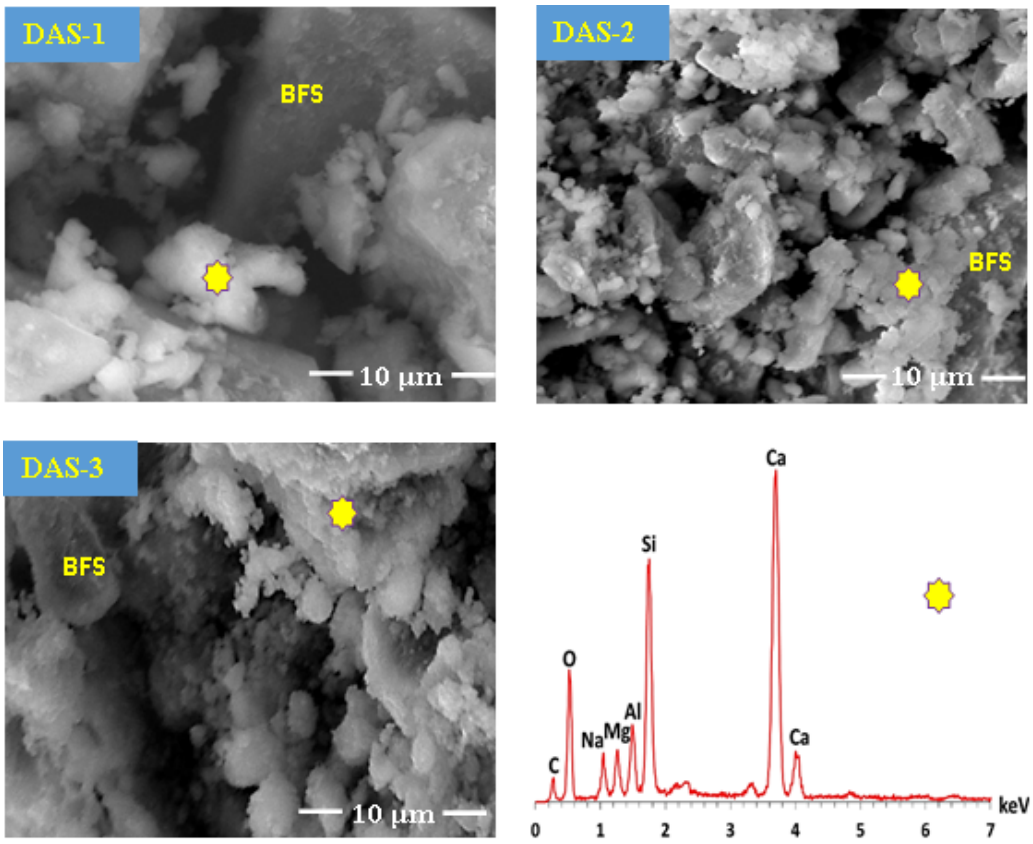

Figure 2

FESEM-micrographs and EDS-analysis of DAS-powders containing (a) 1, (b) 2, and (c) 3 wt.% NaOH.

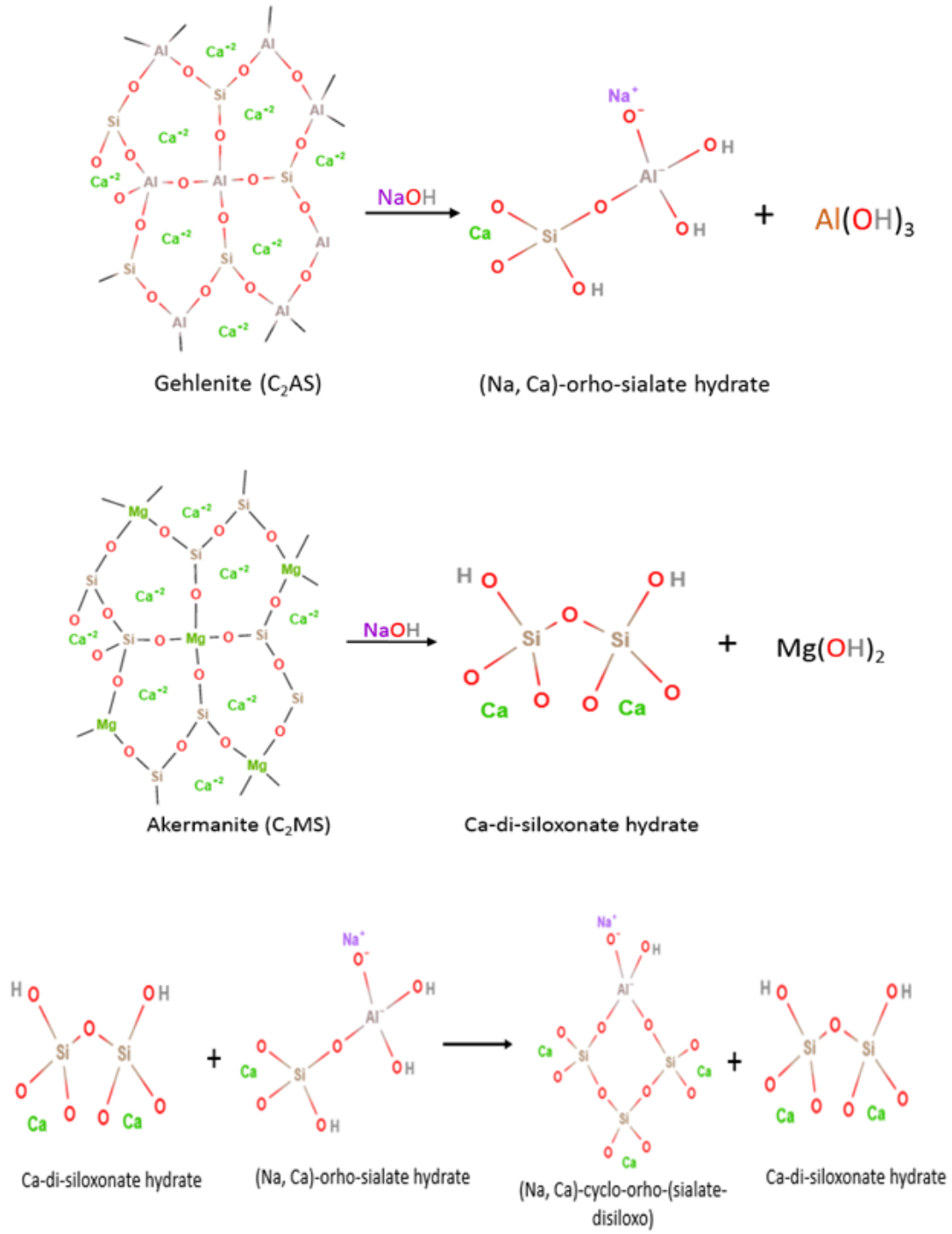

Figure 3

Alkali-activation mechanism of BFS adapted from Davidovits [44].

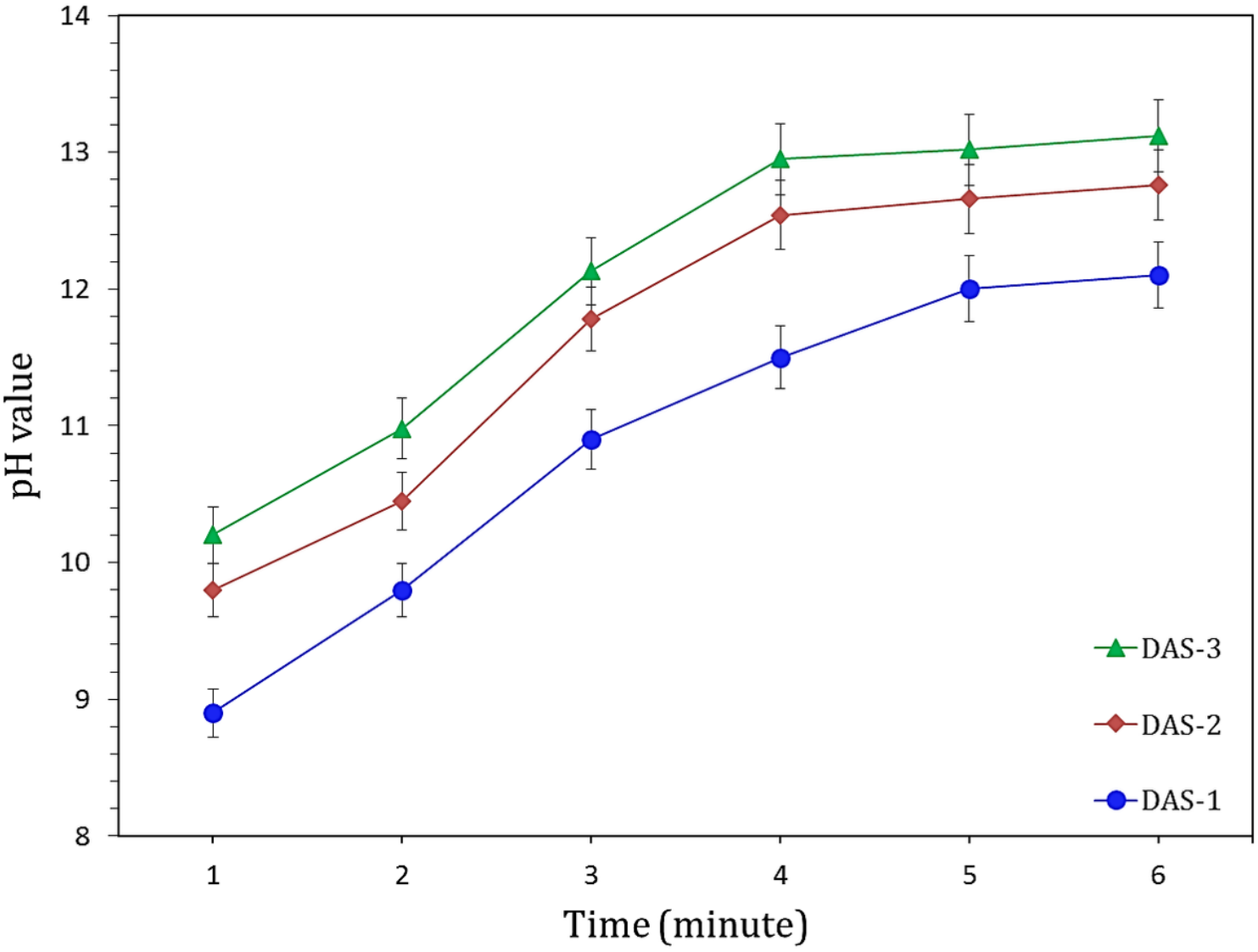

Figure 4

pH-values of leachates of dry activator powders.

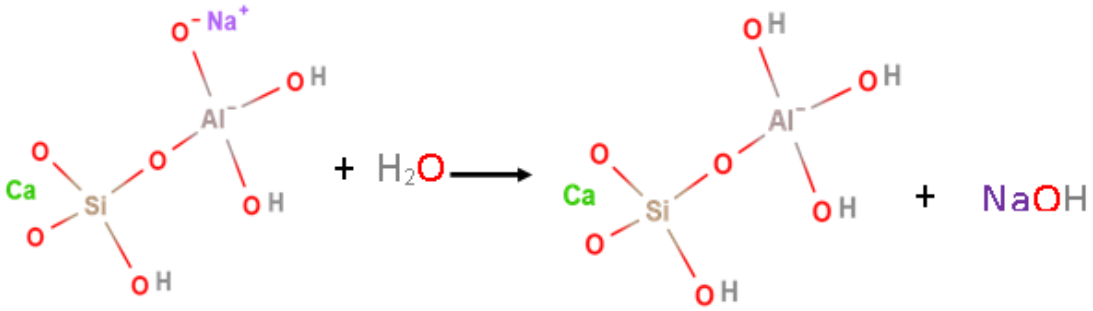

Figure 5

Interaction of activated species within dry activator powder with water.

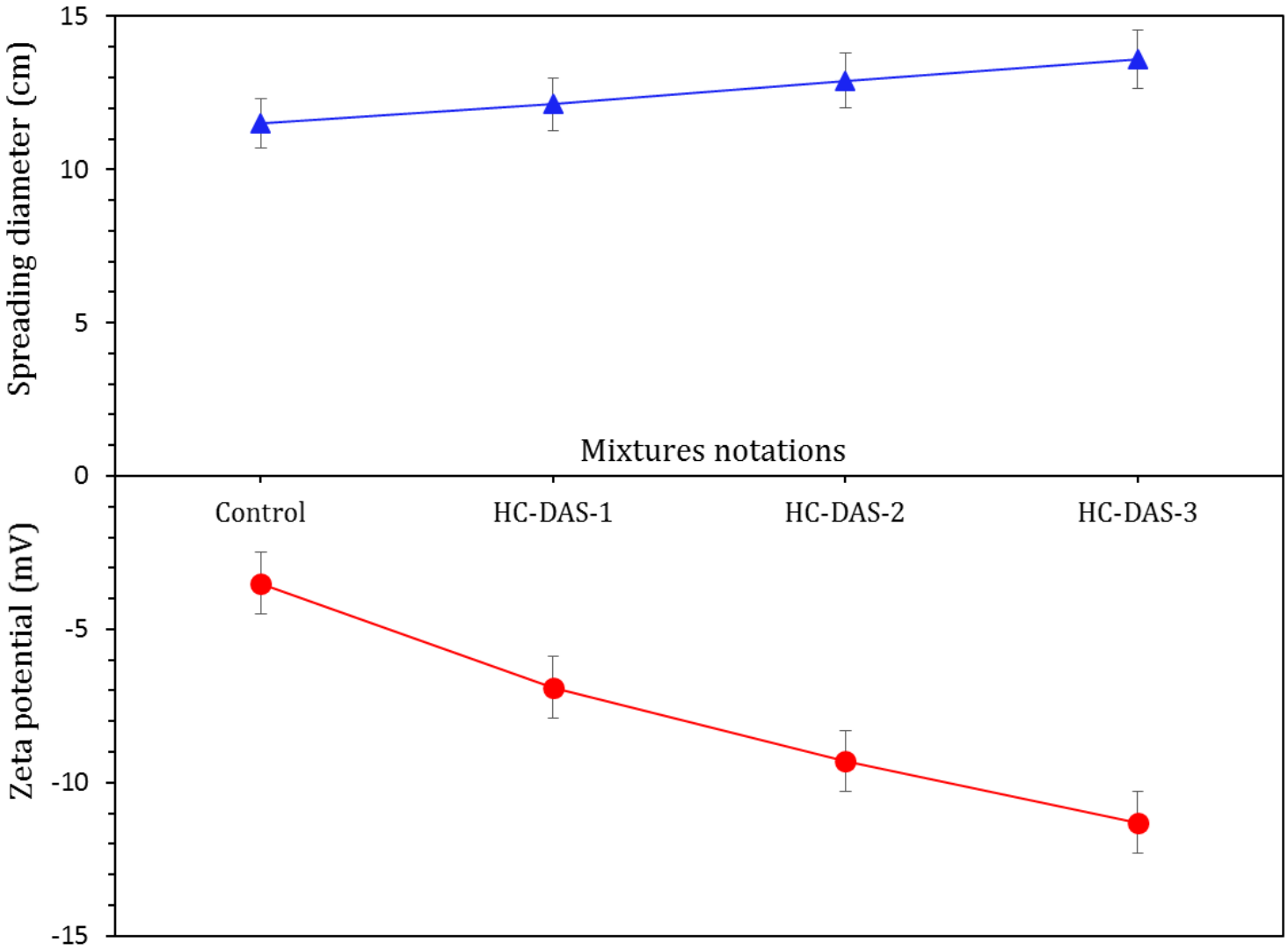

Figure 6

Workability and zeta potential of the fresh control and one-part-HC mortars.

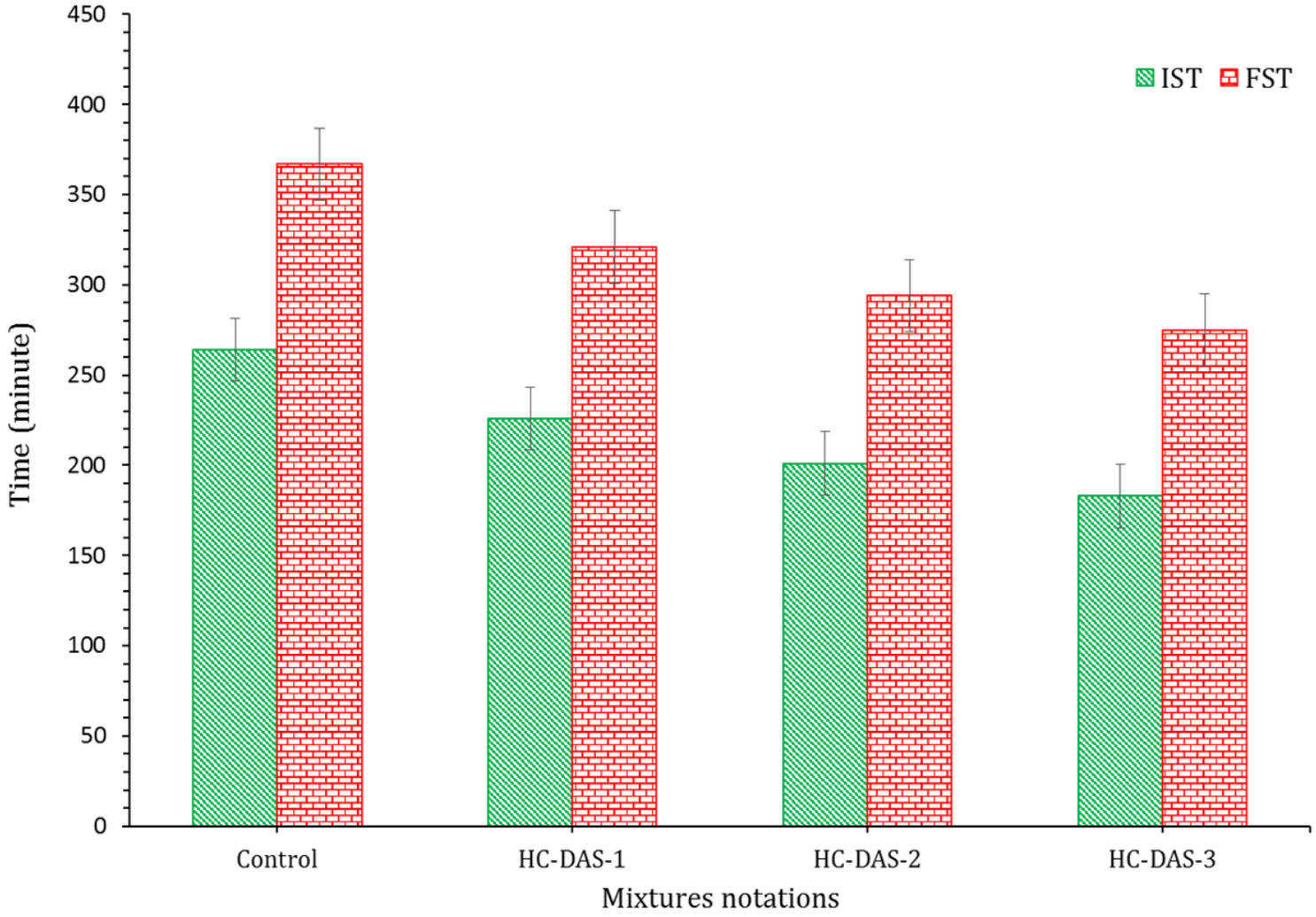

Figure 7

Setting time of the fresh BFS-OPC and one-part-HC pastes.

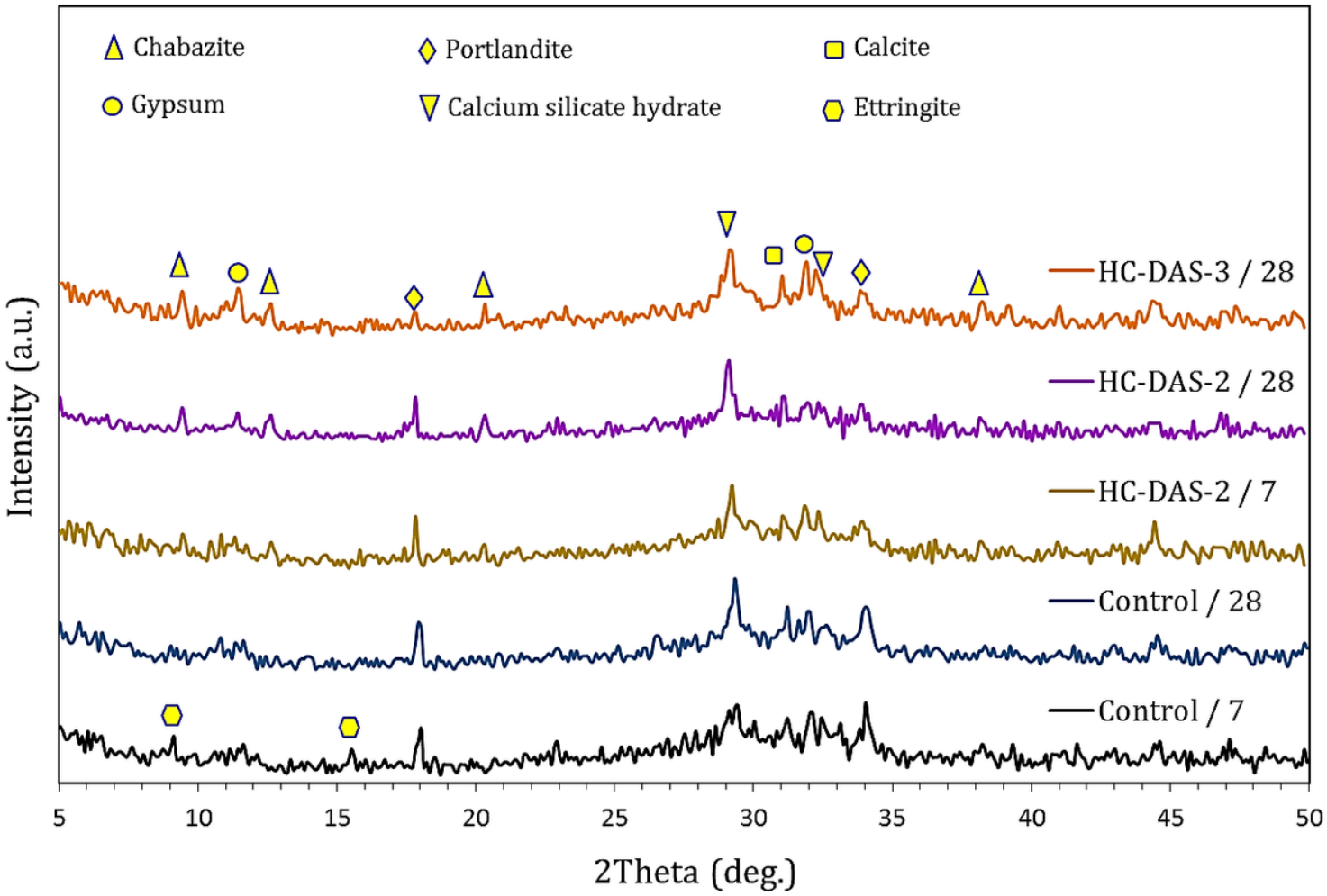

Figure 8

XRD-patterns of control sample and HC-DAS-2 pastes at 7 and 28 days as well as HC-DAS-3 mixture at 28 days of curing.

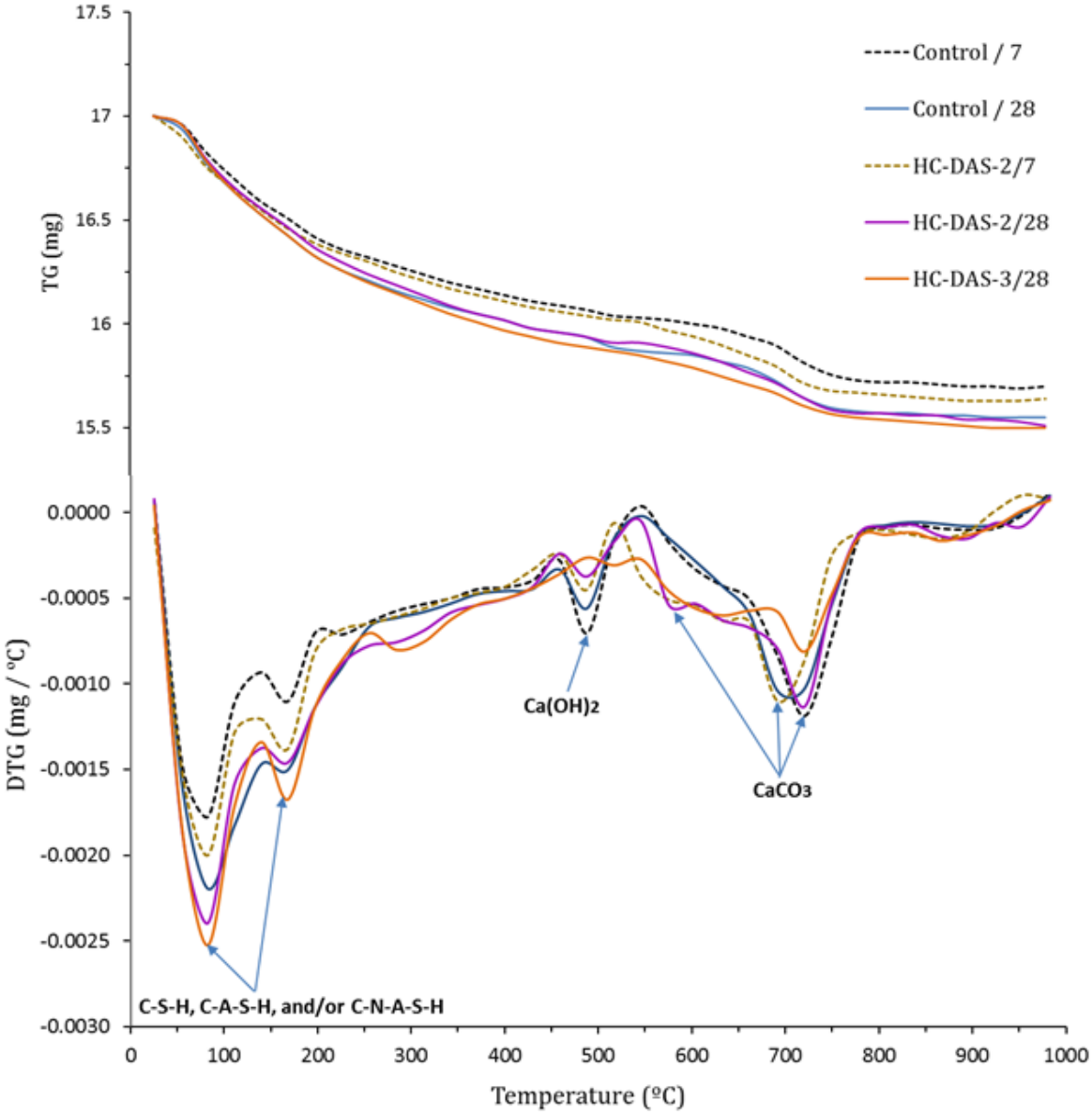

Figure 9

TG/DTG-curves of control sample and HC-DAS-2 pastes at 7 and 28 days as well as HC-DAS-3 mixture at 28 days of curing.

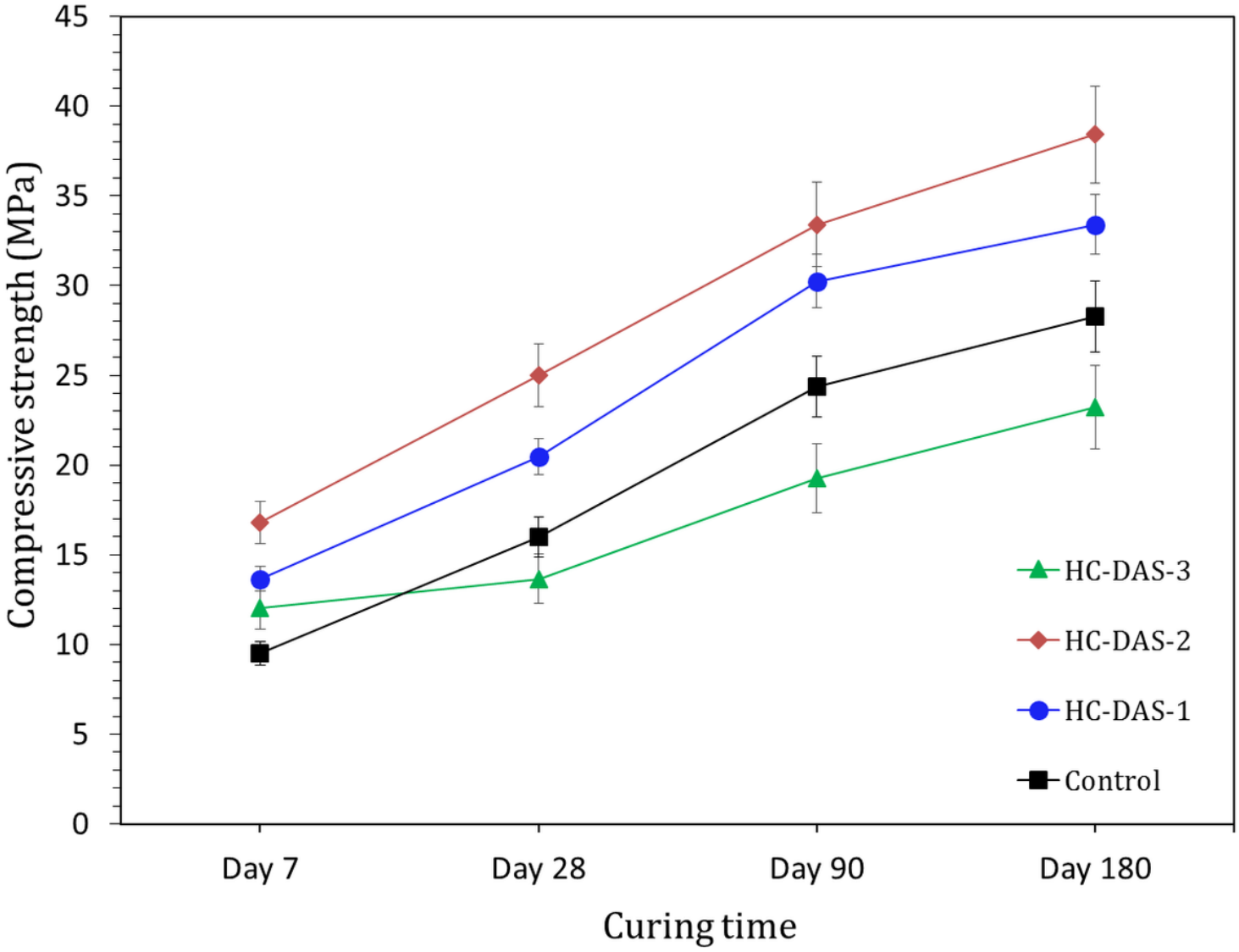

Figure 10

Compressive strength of the hardened BFS-OPC blend and one-part-HC-mortars.

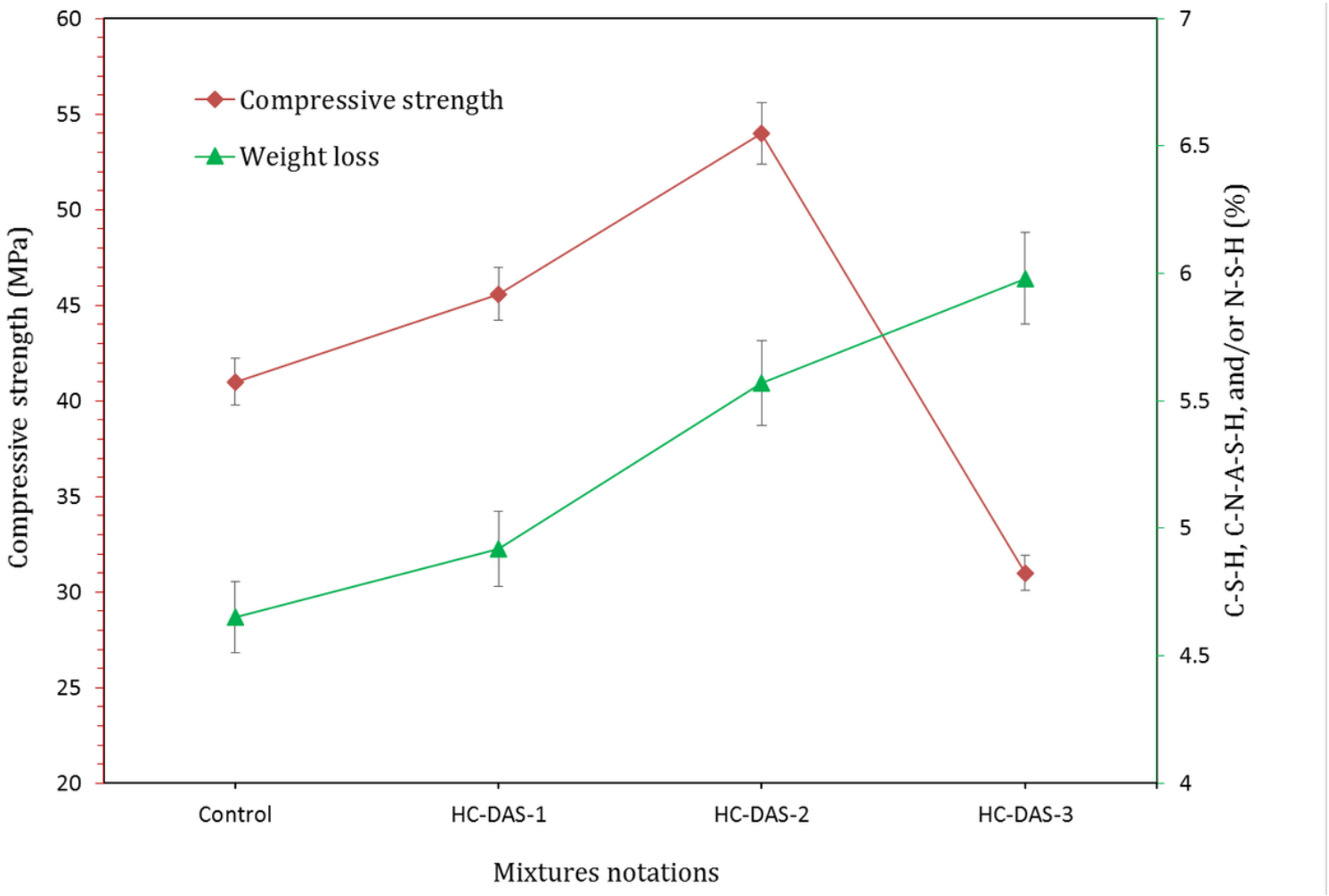

Figure 11

Relationship between weight losses of the hydration products within the hardened cement pastes and the compressive strength.

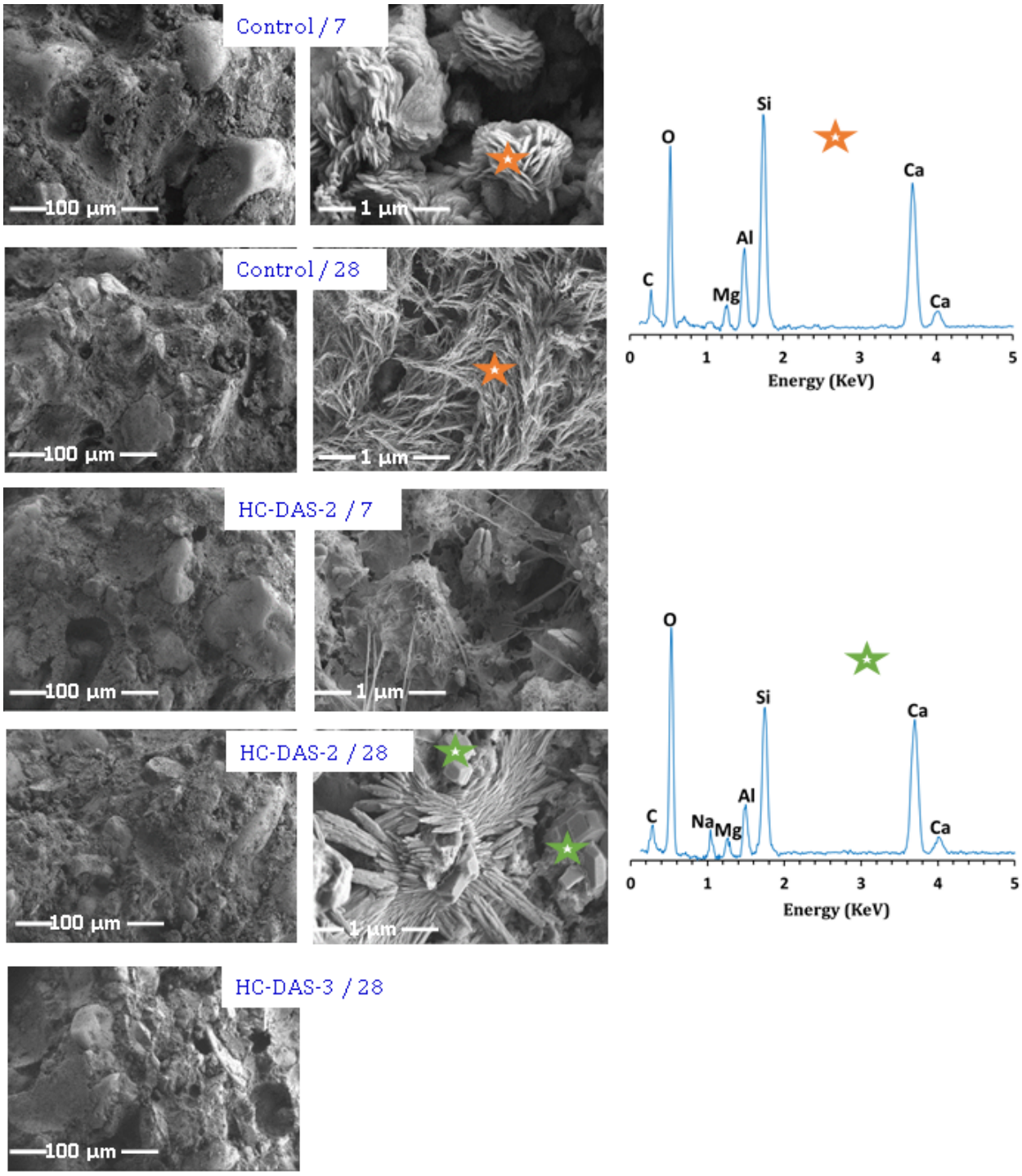

Figure 12

FESEM-micrographs of control sample and HC-DAS-2 mixture at 7 and 28 days of curing as well as HC-DAS-3 mixture at 28-days of curing.

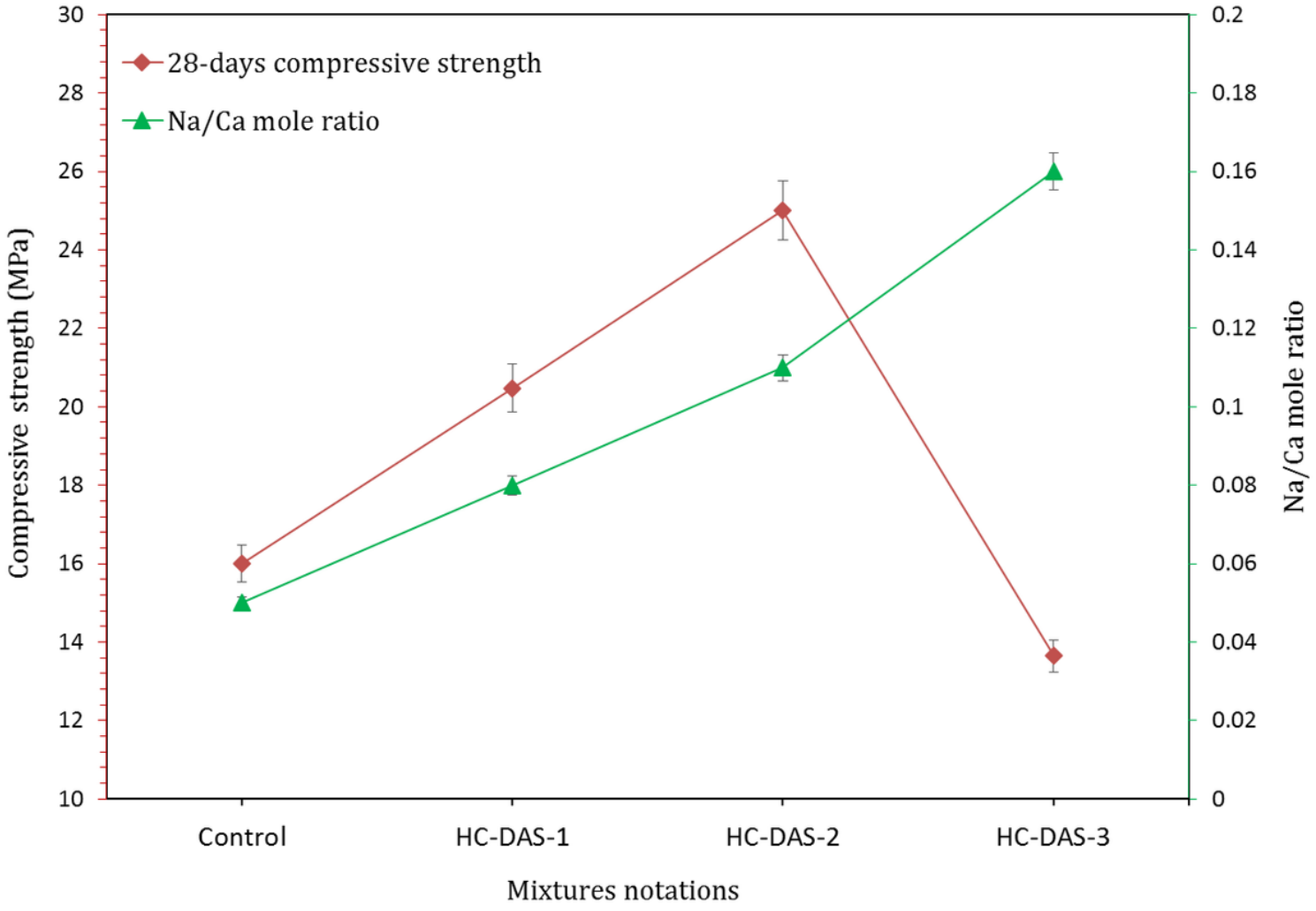

Figure 13

Relationship between Na/Ca ratio and compressive strength of the 28-days hardened mortars having different DAS contents